Eur. Phys. J. B **34**, 479–487 (2003)
DOI: 10.1140/epjb/e2003-00247-7

THE EUROPEAN PHYSICAL JOURNAL B

Fractal geometry of critical Potts clusters

J. Asikainen[1,a], A. Aharony[2], B.B. Mandelbrot[3], E. Rausch[3], and J.-P. Hovi[2,3]

[1] Helsinki Institute of Physics and Laboratory of Physics, Helsinki University of Technology, Finland
[2] Raymond and Beverly Sackler Faculty of Exact Sciences, School of Physics and Astronomy Tel Aviv University, Ramat Aviv 69978, Tel Aviv, Israel
[3] Department of Mathematics, Yale University, New Haven, CT 06520-8283, USA

Received 4 December 2002 / Received in final form 2 June 2003
Published online 9 September 2003 –

Abstract. Numerical simulations on the total mass, the numbers of bonds on the hull, external perimeter, singly connected bonds and gates into large fjords of the Fortuin-Kasteleyn clusters for two-dimensional q-state Potts models at criticality are presented. The data are found consistent with the recently derived corrections-to-scaling theory. A new method for thermalization of spin systems is presented. The method allows a speed up of an order of magnetization for large lattices. We also show snapshots of the Potts clusters for different values of q, which clearly illustrate the fact that the clusters become more compact as q increases, and that this affects the fractal dimensions in a monotonic way. However, the approach to the asymptotic region is slow, and the present range of the data does not allow a unique identification of the exact correction exponents.

PACS. 05.50.+q Lattice theory and statistics (Ising, Potts, etc.) – 05.45.Df Fractals – 75.10.-b General theory and models of magnetic ordering – 75.40.Cx Static properties (order parameter, static susceptibility, heat capacities, critical exponents, etc.)

1 Introduction

q-state Potts models have played an important role in condensed matter physics [1]. Here we study geometrical aspects of the critical Potts clusters, in two dimensions. The q-state Potts model [2] is defined through the Hamiltonian

$$\mathcal{H} = -K \sum_{\langle i,j \rangle} (\delta_{\sigma_i,\sigma_j} - 1), \tag{1}$$

where $\langle i,j \rangle$ denotes the summation over nearest neighbor sites i,j, the spin variable σ_i can take any of the values $1,2,\ldots,q$ and K is the thermal coupling with the factor $1/k_{\mathrm{B}}T$ absorbed in it. It is possible to extend q to real values [1], but here we concentrate on the Potts model with integer values of q. In particular, we study Potts models with $q = 1,2,3$, and 4, where the thermal phase transition at the critical inverse temperature $K_c = \ln(1+\sqrt{q})$ [1] is of second order. Below we present simulations at $K = K_c$.

One defines the fractal clusters in the Potts model through the Fortuin-Kasteleyn (FK) [3] cluster decomposition, which states that the model can be mapped onto a general percolation model. The partition function of the Potts model $\mathcal{Z} = \mathrm{Tr}_\sigma e^{\mathcal{H}}$ can be expressed in terms of bond variables as $\mathcal{Z} = \mathrm{Tr}_{\mathrm{bonds}} p^b (1-p)^n q^{N_c}$, where b is the number of bonds and n is the number of interactions that did not form a bond in a configuration with N_c clusters [4]. Here, $p = 1 - e^{-K}$, and $\mathrm{Tr}_{\mathrm{bonds}}$ means a summation over bonds. Thus, the problem of a thermal lattice model can be mapped to a graph problem. The FK decomposition has been the starting point for efficient cluster algorithms [4,5] for simulation of spin models.

The Potts model has been shown to exhibit a rich critical behavior, and it has been related to a number of problems in lattice statistics [1]. Although of great theoretical interest in itself, it also has many experimental realizations. The 1-state Potts model is equivalent to a bond percolation problem [1], and the 2-state Potts model is the same as the Ising model [6]. The $q = 3$ Potts model has been shown to describe absorbed monolayers on two-dimensional (2D) lattices [7,8]. Domany *et al.* [9] suggested that N_2 absorbed on krypton-plated graphite should exhibit the same critical behavior as the $q = 4$ Potts model. More references on the experimental realizations can be found in the review article by Wu [1].

In this work we study geometrical aspects of the critical Potts clusters in two dimensions. This is in direct analogy with the geometry of percolation clusters, which has been widely studied [10–18]. Specifically, we measure the fractal dimensions D_M, D_H, D_{EP}, D_{SC}, and D_G describing the scaling of the cluster's mass, hull, external accessible perimeter, singly connected bonds and the gates to *narrow-gate* fjords, respectively, with its radius of gyration R.

In the case of percolation, D_{SC} was first discussed by Coniglio [11,12], and measured by Pike and Stanley [13].

[a] e-mail: joonas.asikainen@inf.ethz.ch

Table 1. Exact theoretical predictions. Superscripts refer to following articles: [a] Saleur and Duplantier [19], [b] Duplantier [20], [c] Cardy *et al.* [23], [d] den Nijs [26], [e] Aharony and Asikainen [21].

	D_S	$q=1$	$q=2$	$q=3$	$q=4$	c_S/a
g		$\frac{8}{3}$	3	$\frac{10}{3}$	4	
M^{a}	$(g+2)(g+6)/(8g)$	$\frac{91}{48}$	$\frac{15}{8}$	$\frac{28}{15}$	$\frac{15}{8}$	$\frac{1}{16}$
H^{a}	$1+2/g$	$\frac{7}{4}$	$\frac{5}{3}$	$\frac{8}{5}$	$\frac{3}{2}$	$-\frac{1}{4}$
EP^{b}	$1+g/8$	$\frac{4}{3}$	$\frac{11}{8}$	$\frac{17}{12}$	$\frac{3}{2}$	$\frac{1}{4}$
SC^{a}	$(3g+4)(4-g)/(8g)$	$\frac{3}{4}$	$\frac{13}{24}$	$\frac{7}{20}$	0	-1
θ^{c}	$4(4-g)/g$	2	$\frac{4}{3}$	$\frac{4}{5}$	0 (log)	
θ'^{d}	$4/g$	$\frac{3}{2}$	$\frac{4}{3}$	$\frac{6}{5}$	1	
θ''^{e}	$2/g$	$\frac{3}{4}$	$\frac{2}{3}$	$\frac{3}{5}$	$\frac{1}{2}$	

D_H was defined by Mandelbrot [14] and first measured by Voss [15], while theoretical arguments were proposed by Bunde and Gouyet [16]. D_{EP} was invented and measured by Grossman and Aharony [17]. The quantity D_G has only been discussed theoretically by Aizenman *et al.* [18].

In the case of the Potts model for general values of q, analytical expressions for the exponents D_M, D_H and D_{SC} were given by Saleur and Duplantier [19]. Finally, the analytical form of the exponents D_{EP} was given by Duplantier [20]. The available theoretical values of the exponents are summarized in Table 1, in terms of the Coulomb gas coupling constant

$$g = \frac{4}{\pi} \arccos\left(-\frac{\sqrt{q}}{2}\right). \tag{2}$$

Although there exists much numerical work on the percolation clusters (*i.e.* $q = 1$), we are not aware of any detailed numerical study of most of the above mentioned quantities for $q > 1$, and especially when q approaches the critical value $q_c = 4$.

Section 2 describes the numerical methods used in the simulation of the Potts models. We also introduce a new method for thermalization of the spin lattices. Our numerical simulations show that the asymptotic power law dependence of the various masses on R is approached relatively slowly, and therefore the analysis of the data must include *correction terms*, particularly as q approaches q_c. The theory developed to obtain these correction terms [21] is briefly summarized in Section 3. We compare our numerical data with the exact predictions in Section 4. Finally, we present the summary and conclusions in Section 5.

2 Simulation

Numerical simulations of spin models have developed from the local spin flip type algorithm [22] to the more advanced cluster algorithms [4,5]. Our simulations were done on a 2D square lattice with both open and periodic boundary conditions. Clusters of the q-state Potts model were generated using the Swendsen-Wang algorithm [4], which is based on the cluster decomposition by Fortuin and Kasteleyn [3]. The size of the system in our simulations was 4096^2 spins for all q. Figure 1 shows sample clusters for different values of q.

Figure 1 already gives a qualitative summary of our results. Just by looking at this figure, one can see the monotonic variation of the shapes of the clusters with q: as q increases, there are less singly connected sites, and the external boundary of the cluster becomes smoother. All of these qualitative features are consistent with the theoretical predictions in Table 1.

All simulations were started with a homogeneous initial condition, with all spins initially parallel to each other. First we thermalized the system to allow the model to equilibrate. Thermalization was checked by measuring both the energy per spin e, directly from the Potts Hamiltonian, and the magnetization per spin m, using the representation of Potts spins in a $q-1$ dimensional space [1].

Thermalization of large spin systems takes a very long time. The quantities of interest in this work show a relatively slow approach to the asymptotic values. Thus, extremely large lattices are required for the analysis of the scaling behavior of the cluster subset masses. When performing simulations on lattices of linear size $L = 2^{12} = 4096$, about 20 000 Monte Carlo steps (lattice sweeps) are needed to equilibrate the system.

We devised a simple method to overcome the problem with long thermalization times. We started the thermalization with a small lattice of size L_1 and thermalized it. We then periodically copied the spin configuration of the small lattice to a lattice with twice as large a size, $L_2 = 2 \times L_1$, and thermalized it. We continued this process until the desired system size was reached. In practice, it is recommended to compare the values of e and m obtained this way with the values obtained from conventional thermalization to be sure that the system is really thermalized. Alternatively, one can continue running the simulation and collect the values of thermodynamical variables as a function of time and check that there is no increasing or decreasing trend in them. The thermalization method described above allows a speed-up by an order of magnitude in thermalization for a Potts spin system of 1024^2 spins. This thermalization method is one of the new elements in the present paper.

After the spin system was thermalized, we took samples of the cluster configurations after every 20 spin updates (corresponding roughly to the correlation time for the present system sizes) to get uncorrelated samples. Each cluster of the present configuration was taken separately under investigation. However, as a precaution to avoid some of the finite size effects, we collected the data only from those clusters which did not involve spins on

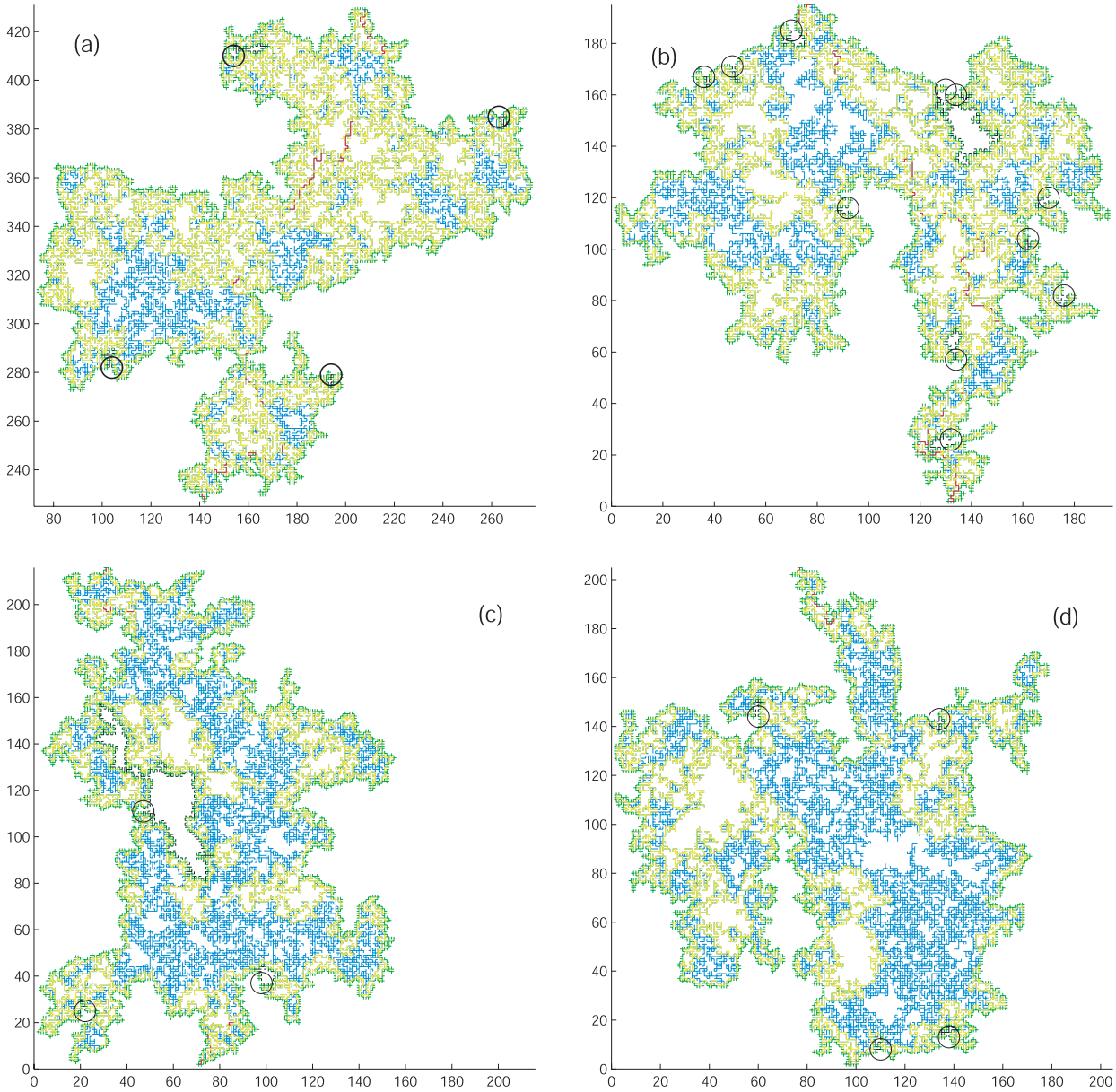

Fig. 1. Computer generated Potts clusters for (a) $q = 1$, (b) $q = 2$, (c) $q = 3$ and (d) $q = 4$ state Potts models. Colors indicate different subsets: SC bonds are shown in red, H bonds are shown in yellow and the rest of the bonds contributing to M are shown in blue. The EP bonds are colored green and the gates to fjords are marked by black circles, while the fjord is shown with a black line. For all the clusters, the total masses M_M are in the range $14400 - 17600$. Note the decrease of D_H with q.

the boundary. For the remaining clusters we determined the masses of the cluster subsets. The total mass of the cluster is defined as the number of occupied bonds in the cluster. The number of bonds belonging to the hull, external perimeter and the number of singly connected bonds were counted using directed walkers that walk on the appropriate cluster perimeter [10,17].

To measure the number of gates to fjords of different gate sizes (S_G) a walk was initiated on the EP. The walker starts from the left vacant neighbor of the lower-left site belonging to the cluster and goes around the cluster on the EP always trying to turn to the right. At each site, we look at the neighbors on the left hand side and check whether the sites within a predefined distance S_G belong to the EP or not. If the sites (and bonds) up to the distance S_G are not EP sites and the site at the distance S_G belongs to the EP, the walker is about to enter a fjord with a gate size S_G. All fjords with different gate sizes were counted during a single walk around the cluster with an array of boolean variables that indicate whether the walker is within a fjord of given size. If the walker was in a fjord of a gate size S_G, fjords with gate size $S'_G > S_G$ were not allowed in the statistics. In practice, all measured values of S_G gave similar results, and we report only the results for $S_G = 1$.

As noted by Aizenman *et al.* [18], the scaling concerns fjords whose size L_F is comparable to that of the

cluster, R, and whose gate's width is much smaller than L_F. The reason for this is easy to understand, since small kinks and pits are a natural part of the fractal cluster's perimeter. Thus, only large enough fjords were included in the statistics. This was taken into account by choosing a suitable parameter $s \in [0.1, 0.2]$, and counting only fjords with $L_F > sR$.

Since any thermalized spin configuration contains clusters of many sizes, we collected the data in multiplicatively increasing bins of the size of the cluster. Each bin contained the clusters of sizes within $[R_i, R_{i+1} = \sqrt{2}\ R_i]$.

3 Corrections to scaling

In our recent publication [21], we derived theoretically the *corrections-to-scaling* terms for the various cluster subset masses. The corrections arise from three different sources: (a) using the renormalization group approach, (b) mapping to the coulomb gas, and (c) considering the uncertainty of the correct measure for the linear cluster size, which implies corrections of the order of $1/R$.

The first correction relates to the *dilution* field ψ, which is generated under renormalization even when one starts with the non-diluted case [23]. Solving the renormalization group recursion relations (RGRR's) for $\psi(\ell)$, where ℓ is the scale variable, substituting the solution to the RGRR's for the field h_S conjugate to the density $\rho_S = M_S/R^d$ and finally calculating the scaling of the density $\rho_S(\ell)$ with the cluster's linear size $R = e^\ell$ yields the following predictions for the approach of each mass M_S to the asymptotics. Here, $S = M,\ H,\ EP$ or SC.

In the $q = 4$ case, the renormalization group calculation is exact, yielding logarithmic corrections to the scaling of $M_S(R)$:

$$M_S \propto R^{D_S} \left(\log R + B \log(\log R) + E\right)^{-c_S/a} \times \left(1 + \mathcal{O}(\log\log R/\log R)\right), \quad (3)$$

with $D_S = y_S(q = 4)$ and c_S/a as given in Table 1 (see below). Note that B is universal, and the non-universal constant E is the same for all S. Equation (3) generalizes the logarithmic corrections of Cardy *et al.* [23].

We were recently directed to a previous study by Vanderzande and Marko [24], in which they considered corrections to scaling for magnetic and percolative susceptibilities in the $q = 4$ Potts model. They construct RGRR's from which the logarithmic corrections to the cluster's total mass could be obtained, in agreement with our analytical calculations [21].

For $q < 4$, to leading order in $\epsilon' = \sqrt{4 - q}$, the same procedure yields

$$M_S \propto R^{D_S} \left(1 - \hat{B} R^{-\theta}\right)^{-c_S/a} \approx R^{D_S} \left(1 + f_S R^{-\theta}\right), \quad (4)$$

where $D_S \approx y_S - c_S\epsilon'$ and $\theta \approx 2a\epsilon'$. Note that to the lowest order in ϵ', the ratios $f_S/f_{S'}$ are universal, being equal to $c_S/c_{S'}$. This is similar to analogous ratios for thermodynamic properties in the usual ϵ-expansion [25]. This universality should hold to all orders in ϵ'. Expanding the exact D_S (Tab. 1) in ϵ' yields c_S. Using also $a = 1/\pi$ [21,23] yields our predictions for c_S/a (given in Tab. 1), to be used in the fitting procedure.

The second source of corrections involves new contributions to the relevant pair correlation functions in the Coulomb gas representations. Den Nijs [26] derived such corrections to the order parameter correlation function. Since correlation exponents x are related to the fractal dimension *via* $D = d - x$, the correction exponents can be related to the corresponding correction terms for the scaling of the mass M_M, yielding the leading correction

$$\theta' = 4/g, \quad (5)$$

where g is the (q-dependent) Coulomb Gas coupling constant (see Eq. (2) and Tab. 1).

Using a similar approach we found in the case of the hull and the singly connected bonds that the leading correction exponent is given by

$$\theta'' = 2/g. \quad (6)$$

We argued that this correction would also hold for the external perimeter [21].

The last source of corrections involves 'analytic' terms, coming *e.g.* from linear cuts with dimensions $(D_S - 1)$, [27] or from replacing R by $(R + A)$, since there are many possible candidates for the correct linear measure of the cluster. These would imply corrections of relative size $1/R$.

4 Results

We now present the numerical data from large scale Monte Carlo simulations of the Potts models. Our aim is to confirm the exact predictions of the fractal dimensions D_S in the cases where they are available and to give numerical estimates for the exponents that have not yet been calculated exactly. In addition, we want to numerically confirm the corrections-to-scaling theory presented in the previous section.

We obtain good agreement with the theoretically predicted values for most of the fractal dimensions D_S. The worst agreement is found for the exponent of the external perimeter D_{EP} for $q > 2$ Potts models. The reasons for this will be discussed below. However, fixing the correction terms and performing fits only to the amplitudes and to the fractal dimensions D_S in the logarithmic derivatives of equations (3) and (4), yielded estimates for the subset fractal dimensions that agree to the precision of 0.05 or better with the theoretical predictions of Table 1.

As we discuss below, our data are consistent with the theoretical predictions for both the leading and correction exponents; when we fix these exponents, we get very good fits. Attempts to fit without the corrections give bad values for the leading exponents. However, the range of available cluster sizes is not sufficient to allow a general

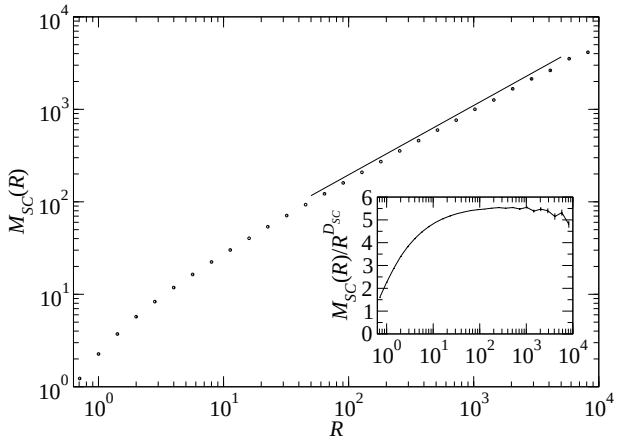

Fig. 2. Site percolation model. The number of the singly connected bonds $M_{SC}(R)$ *vs.* the cluster linear size R. The predicted slope $D_{SC} = 3/4$ is indicated by the solid line. The inset shows the scaled mass $M_{SC}(R)/R^{D_{SC}}$. Note the saturation to the asymptotic scaling at $R \approx 300$.

search for the correction exponents. Therefore, these exponents (θ, θ' (or θ") and c_S/a) were fixed in our fits at their theoretical values, and the fits varied only the respective amplitudes. Thus, we have shown consistency with theory, but we have not proven that this theory uniquely describes the data.

We start this section by studying the fractal geometry of clusters in the site percolation model, which is computationally easier to simulate. The reasons behind the difficulties in the comparison of the numerical data with the analytical predictions are discussed. We then proceed to present our numerical data on the Potts clusters. In all the figures of this section, whenever the error bars are not shown they are smaller than the size of the symbols.

4.1 Site percolation clusters

For $q = 1$ we simulated site percolation on a square lattice of size 24576^2, using the Newman-Ziff cluster labeling [28] which is an improved version of the Hoshen-Kopelman algorithm [29]. Thus the linear lattice size was 6 times larger than in the simulation of Potts clusters with $q \geq 1$.

To get a feeling of what kind of problems are present in the fitting procedure when the theoretically predicted correction terms of equations (3) and (4) are fitted to the numerical data on the cluster subset masses $M_S(R)$, let us consider as an example the scaling of the number of singly connected bonds. Figure 2 illustrates the scaling of $M_{SC}(R)$ with the cluster size R on a double logarithmic scale. The solid line in the main figure indicates the predicted slope. The linear fit to the data on log-log scale yields an estimate for the asymptotic fractal dimension D_S which is less than 0.01 off the exactly known value $D_{SC} = 3/4$.

Although the asymptotic scaling regime $M_{SC}(R) \propto R^{D_{SC}}$ can be seen here, there are difficulties in the extraction of the correction terms of equation (4). The smallest value of R included in the linear fit to the data on $\log - \log$ scale in Figure 2 corresponds to the regime where the influence of the correction terms are about to vanish, thus justifying fitting without any correction terms. The saturation to the asymptotics can be seen more clearly in the inset of Figure 2 where data are scaled with the predicted asymptotic behavior $M_{SC}(R)/R^{D_{SC}}$. The inset shows that at about $R \approx 300$ the correction terms can be neglected in this case. However, at the same point the statistics becomes so noisy, making a precise estimation of the correction terms difficult. An additional difficulty arises from the fact that the finite size of the lattice is not taken into account in any way in the finite size scaling form of equation (4). Due to the finite system sizes, statistics of the large cluster is biased in such a way that only the compact clusters fit in the lattice without touching the boundaries. The extended clusters having for example more EP sites than compact clusters with the same radius of gyration R, are absent. This bias cannot be taken into account by any known correction terms. We tried to extrapolate the data from different system sizes to obtain an asymptotic curve for an infinitely large system, but the statistics is far from sufficient for such a procedure.

4.2 Potts clusters

In the case of Potts clusters, system sizes that can be used in the simulations are much smaller than those in the site percolation case, since in addition to the spin variables, also bonds must be stored in the computer memory. This causes the finite size effects to be even more pronounced than those present in the site percolation model simulations. In addition, the correction exponents in the $1 < q < 4$ Potts models are smaller than those in the $q = 1$ case. Also, the logarithmic corrections present in the 4-state Potts model are weaker than any of the power law corrections in $q < 4$ models. Thus, the influence of the corrections-to-scaling terms extends to much larger values of R.

The data analysis was done by fitting the theoretical predictions of Section 3 to the data. The nonlinear fitting was done using the Levenberg-Marquardt method [30]. The measure for the quality of fits is χ^2. Values of χ^2 close to one indicate a good fit.

We found that for $q < 4$, fitting directly to the mass gave better fits (in terms of χ^2). Thus, for illustrational purposes in the $q < 4$ case, we show below some fits done directly to the mass

$$M_S/R^{D_S} = E_S(1 + f_S R^{-\theta} + f'_S R^{-\theta'} + g_S/R), \qquad (7)$$

where E_S, f_S, f'_S, g_S are fitting amplitudes, while θ and θ' and D_S come from theory.

To get the numerical estimate for the fractal dimensions, we perform fits to the logarithmic derivative of equation (7):

$$D_S^{\text{eff}}(R) = D_S + f_S R^{-\theta} + f'_S R^{-\theta'} + g_S/R, \qquad (8)$$

with parameters similarly as in (7).

In the $q = 4$ case, the fits were done to

$$D_S^{\rm eff}(R) = d\log M_S/d\log R \approx D_S - \frac{(c_S/a)(B + C + \log R)}{(C + \log R)(E + \log R + B\log(C + \log R))} + Z/\log R. \quad (9)$$

Note that we have replaced the $\log\log R$ term in equation (3) by the more general $\log(C + \log R)$. Also, the logarithmic derivative of the higher order term on the RHS of equation (3) was approximated by a simpler form $1/\log R$. In the fitting procedure, the possibility of having many candidates for the correct linear measure of the cluster size was taken into account by allowing R to adjust to $R + A$ (see Sect. 3). When fitting to equation (3), only the parameter c_S/a is fixed, while the rest (D_S, A, B, C, E and Z) are allowed to fit.

Below, the results of our numerics are summarized for the various subsets. We do not go into the details of numerical estimates for the various amplitudes in the nonlinear fits, since due to the relatively small range of the data and many fitting parameters the estimated error bars are large, and allow no comparison with, for example, the predicted amplitude ratios. Also, precise estimation of the correction exponents θ, θ' (or θ'') as well as the parameters c_S/a is impossible with the presently available range of data.

Instead, we keep the correction exponents (or parameters) fixed and try to extrapolate the fractal dimensions D_S, and to demonstrate that the predicted forms of scaling in equations (7) and (9) are consistent with our numerical data. Specifically, for $q < 4$, in fits to equation (8) θ and θ' (or θ'') were kept fixed at the predicted values. In the $q = 4$ case, only c_S/a was fixed in equation (9). Although there are many fitting parameters as compared to the available range of data, we would like to point out that the fits are rather stable. We checked confidence levels on our estimates to the fractal dimensions D_S by Monte Carlo sampling of the original data within the error bars of each data point (see *e.g.* Chapter 15.6 in [30]). Figure 3 illustrates a confidence level of 99%.

We also estimated the error bars of the fractal dimensions D_S in the following way. First, the numerical estimate for D_S was obtained from the nonlinear fitting procedure with the exactly known correction parameters fixed. Second, the range within which χ^2 did not change more than $\Delta\chi^2 = 1$ was determined by fixing D_S to values in the neighborhood of the original estimate and allowing the other parameters to fit. We feel that it is important to include also this latter analysis in the error bar estimation process, as fixing D_S beyond the range deduced from the confidence level analysis still yields fits with a good value of χ^2.

The logarithmic corrections are most important for the singly connected bonds at $q = 4$, where theory predicts that $D_{SC} = 0$ (see Tab. 1). Indeed, the solid line in Figure 4 shows that a fit to equation (9) isconsistent with this theoretical prediction. In contrast, a fit with a single power law correction term $\theta = 1/2$ (dashed line in Fig. 4) extrapolates to a wrong value near $D_{SC} = 0.21$!

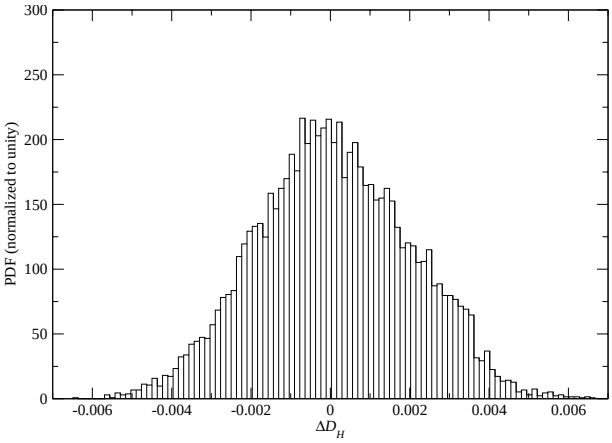

Fig. 3. Probability distribution function (PDF) for finding an estimate for the fractal dimension D_H that deviates by amount ΔD_H in the $q = 4$ case. Histogram was obtained by sampling 10 000 synthesized data sets.

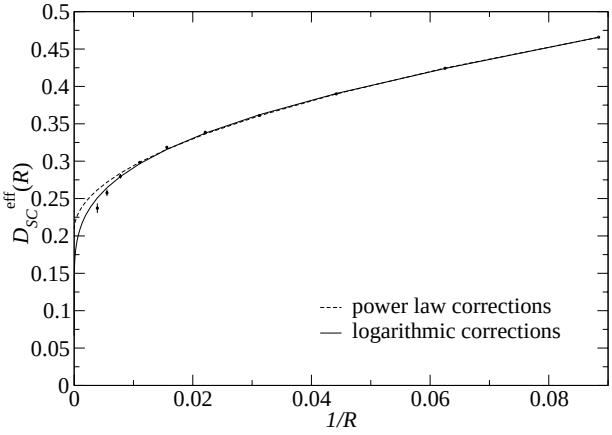

Fig. 4. Example of different fits in the $q = 4$ Potts model to $M_{SC}(R)$. The dashed line shows a fit with a single power law correction ($\theta = 1/2$) and the solid line shows the fit to the logarithmic form of equation (9). Note the difference in the extrapolation to the $R \to \infty$ where the fits give $D_{SC} = 0.21 \pm 0.01$ with a single power law correction term whereas $D_{SC} = 0.03 \pm 0.08$ with the logarithmic form.

4.2.1 Mass

Figure 5 shows an example of the fit to the curve $M_M(q = 3)/R^{D_M}$. The value $\chi^2 = 1.17$ indicates that equation (7) gives a good representation of the data. Our numerical estimates for the fractal dimensions $D_M(q)$, determined as the range of values for which one has $\chi^2 < 2$, are 1.90 ± 0.01, 1.87 ± 0.01, 1.85 ± 0.02 and 2.05 ± 0.15 for $q = 1, 2, 3, 4$, respectively. These are in good agreement with the theoretical predictions.

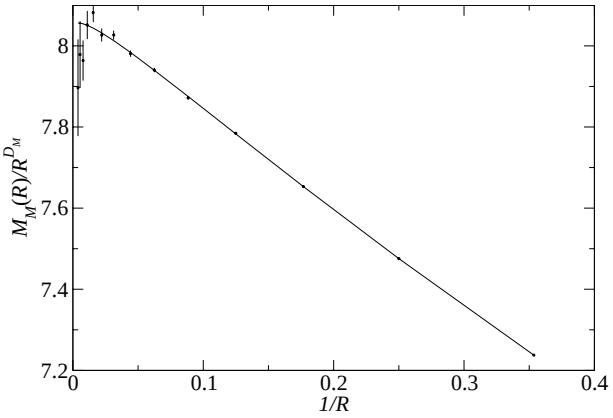

Fig. 5. Total mass of the cluster mass M_M in the 3-state Potts model. Solid line is the nonlinear fit to the data. For this particular fit $\chi^2 = 1.17$.

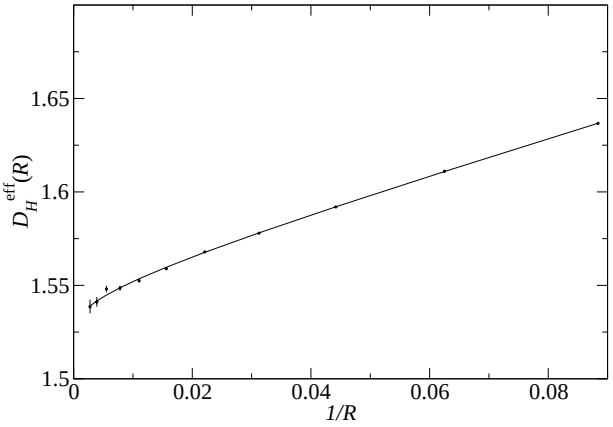

Fig. 6. Effective exponent $D_H^{\rm eff}(R)$ against $1/R$ in the $q = 4$ Potts model. For the fit indicated by the solid line we find $\chi^2 = 1.11$.

4.2.2 Hull

Figure 6 shows a fit to the number of the bonds belonging to the hull in the $q = 4$ Potts model. The value of $\chi^2 = 1.11$ indicates that equation (9) fits the data well. Our numerical estimates for the fractal dimensions $D_H(q)$ are 1.75 ± 0.01, 1.66 ± 0.01, 1.59 ± 0.03 and 1.50 ± 0.01, for $q = 1, 2, 3, 4$, respectively. Agreement with the theoretical predictions is excellent as can be seen by comparison with the values in Table 1.

4.2.3 External perimeter

Figure 7 shows an example of the fit to the external perimeter data in the $q = 2$ Potts model. This fit yields $\chi^2 = 1.77$, implying a reasonably good agreement with equation (7). Again, in the fits for $q < 4$, θ and θ'' of equation (7) were kept fixed and in the $q = 4$ case, c_{EP}/a was fixed. The numerical estimates 1.33 ± 0.05, 1.36 ± 0.02, 1.40 ± 0.02 and 1.48 ± 0.02 for $q = 1, 2, 3, 4$, respectively, agree with the exact predictions.

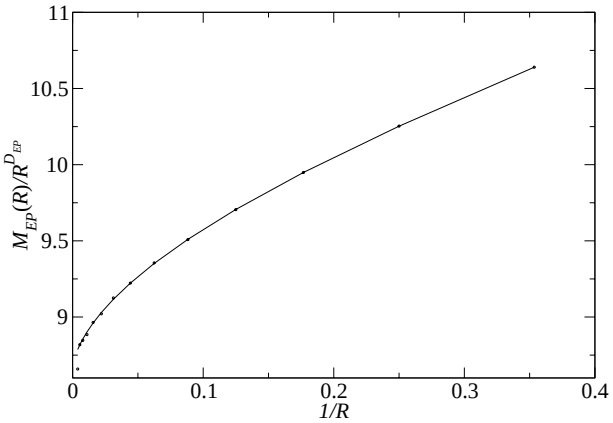

Fig. 7. Number of the external perimeter bonds, M_{EP} *versus* $1/R$ in the $q = 2$ Potts model. Solid line indicates the fit to the data ($\chi^2 = 1.77$).

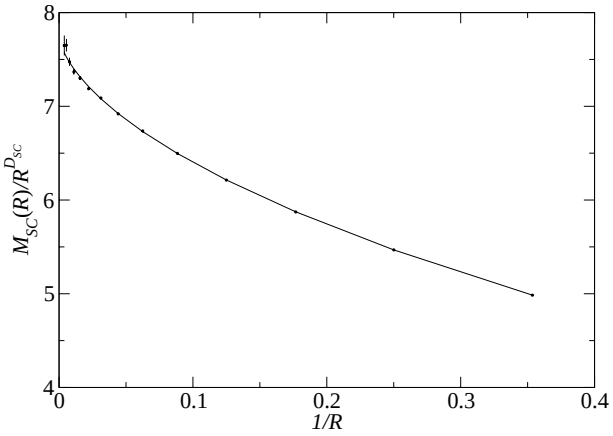

Fig. 8. Number of the singly connected bonds M_{SC} against $1/R$ in the $q = 2$ Potts model. Solid line is the nonlinear fit for which $\chi^2 = 1.21$.

4.2.4 Singly connected bonds

In Figure 8, we show the number of singly connected bonds $M_{SC}(R)/R^{D_{SC}}$ against the cluster size R in the $q = 2$ Potts model. The value $\chi^2 = 1.21$ implies good agreement with equation (7). The numerical estimates for the fractal dimensions are 0.75 ± 0.02, 0.55 ± 0.03, 0.35 ± 0.07, and 0.03 ± 0.08, for $q = 1, 2, 3, 4$, respectively. All the estimates for the fractal dimensions D_{SC} are in good agreement with the theoretical predictions. However, the large value of $\chi^2 \approx 3$ in the $q = 4$ case indicates some discrepancy between equation (9) and the data.

4.2.5 Gates to fjords

Figure 9 shows our numerical data for the number of gates to narrow-gate fjords. The figure shows fits to the data along with the estimates for the fractal dimensions D_G. Our estimate $D_G(q = 1) = -0.9 \pm .05$ agrees with the exact prediction $D_G = -11/12 \approx -0.92$ [18]. Here, only a linear fit to the data on the double logarithmic scale

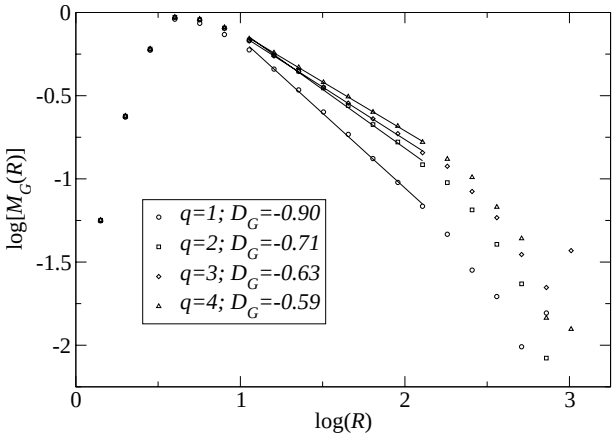

Fig. 9. Data for $M_G(R)$, the number of gates to fjords on log-log scale. Different values of q are represented by the symbols shown in the legends. Straight lines indicate the fits to the data; slopes give the exponents D_G.

Table 2. Comparison of the numerical estimates (n) for the subset fractal dimensions D_S with the exact predictions (e) where available. Uncertainties of the last decimal(s) for each D_S are given in parenthesis.

S	$D_S(q=1)$		$D_S(q=2)$		$D_S(q=3)$		$D_S(q=4)$	
	n	e	n	e	n	e	n	e
M	1.90(1)	$\frac{91}{48}$	1.87(1)	$\frac{15}{8}$	1.85(2)	$\frac{28}{15}$	2.05(15)	$\frac{15}{8}$
H	1.75(1)	$\frac{7}{4}$	1.66(1)	$\frac{5}{3}$	1.59(3)	$\frac{8}{5}$	1.50(1)	$\frac{3}{2}$
EP	1.33(5)	$\frac{4}{3}$	1.36(2)	$\frac{11}{8}$	1.40(2)	$\frac{17}{12}$	1.48(2)	$\frac{3}{2}$
SC	0.75(2)	$\frac{3}{4}$	0.55(3)	$\frac{13}{24}$	0.35(7)	$\frac{7}{20}$	0.03(8)	0
G	−0.90(5)	$-\frac{11}{12}$	−0.71(5)	-	−0.63(5)	-	−0.59(5)	-

was considered, since the scaling regime for the presently available cluster sizes is rather narrow. The parameter s governing the minimal ratio of the fjord size to the cluster size that we used was in the range $0.1 \leq s \leq 0.2$. The actual choice for the value of s does not affect the scaling law, but it merely determines the range where the power law behavior $M_G \sim R^{D_G}$ starts (decreasing s shifts the maximum of the curves $M_G(R)$ to the left). Our numerical estimates for $|D_G(q)|$ decrease with increasing q. Our estimates for $D_G(q)$ are -0.90 ± 0.05, -0.71 ± 0.05, -0.63 ± 0.05 and -0.59 ± 0.05 for $q = 1, 2, 3, 4$, respectively. Our numerical estimates together with the theoretical predictions for all fractal dimensions D_S are summarized in Table 2.

5 Conclusions

The present paper examined the fractal geometry of the Potts clusters at the critical temperature. The aim was to find numerical evidence for the exactly derived subset fractal dimensions D_S [18–20,31] and to give estimates on the dimensions for which there is no exact prediction. We gave the first numerical estimate of the negative fractal dimensions D_G, describing the scaling of the gates to fjords [18].

Analysis of our numerical data revealed a slow and complex approach to the asymptotic behavior. If this is neglected in data analysis, wrong numerical estimates for the dimensions D_S follow. Using the corrections-to-scaling terms derived in our earlier publication [21] in the fitting procedure, excellent agreement with most of the exact dimensions and data was found. The present quality and range of data does not allow a unique quantitative confirmation of the exact correction parameters.

We devised a simple and fast method for thermalization of large spin systems. The method is based on first thermalizing a small sublattice of size L_1, copying it to a larger sublattice of size $L_2 = 2L_1$, and the thermalizing thermalizing the larger lattice. The process is continued until the wanted system size is reached.

We also showed snapshots of the numerically generated Potts clusters for all values of q considered in this paper. The figures already show the qualitative summary of our results, namely the monotonic behavior of the subset masses with increasing values of q.

To summarize, in the comparison between theory and numerics, extreme caution is needed in the extraction of the fractal dimensions D_S from the numerical data. The corrections-to-scaling theory presented already implies that the finite size effects arising from the finite cluster size are strong. In addition, effects coming from the finite lattice size lead to an uncontrollable bias that is very difficult to handle.

We would like to thank Carlo Vanderzande for drawing our attention to their earlier work. We acknowledge support from the German-Israeli Foundation. This work has also been supported in part by the Academy of Finland through its Center of Excellence program. J.A. wishes to thank the Vaisala Foundation for financial support.

References

1. F.Y. Wu, Rev. Mod. Phys. **54**, 235 (1982)
2. R.B. Potts, Proc. Camb. Phil. Soc. **48**, 106 (1952)
3. C.M. Fortuin, P.W. Kasteleyn, Physica (Utrecht) **57**, 536 (1972)
4. R. Swendsen, J. Wang, Phys. Rev. Lett. **58**, 86 (1987)
5. U. Wolf, Phys. Rev. Lett. **62**, 361 (1989)
6. E. Ising, Z. Phys. **21**, 613 (1925)
7. S. Alexander, Phys. Lett. A **54**, 353 (1975)
8. M. Bretz, Phys. Rev. Lett. **38**, 501 (1977)
9. E. Domany, M. Schick, J.S. Walker, Phys. Rev. Lett. **38**, 1148 (1977)

10. D. Stauffer, A. Aharony, *Introduction to Percolation Theory*, revised 2nd edition ed. (Taylor and Francis, Burgess Science Press, Basingstoke, London, 1994)
11. A. Coniglio, J. Phys. A **15**, 3829 (1982)
12. A. Coniglio, Phys. Rev. Lett. **46**, 250 (1981)
13. R. Pike, H.E. Stanley, J. Phys. A **14**, L169 (1981)
14. B.B. Mandelbrot, *The Fractal Geometry of Nature* (W.H. Freedman and Company, New York, 1977)
15. R.F. Voss, J. Phys. A **17**, L373 (1984)
16. A. Bunde, J.F. Gouyet, J. Phys. A **18**, L285 (1985)
17. T. Grossman, A. Aharony, J. Phys. A **19**, L745 (1986)
18. M. Aizenman, B. Duplantier, A. Aharony, Phys. Rev. Lett. **83**, 1359 (1999)
19. H. Saleur, B. Duplantier, Phys. Rev. Lett. **58**, 2325 (1987)
20. B. Duplantier, Phys. Rev. Lett. **84**, 1363 (2000)
21. A. Aharony, J. Asikainen, in *Scaling and Disordered Systems*, edited by F. Family, M. Daoud, H.J. Herrmann, H.E. Stanley (World Scientific, Singapore, 2002); Fractals **11**, 3 (2003); `cond-mat/0206367`
22. N. Metropolis *et al.*, J. Chem. Phys **21**, 1087 (1953)
23. J.L. Cardy, M. Nauenberg, D.J. Scalapino, Phys. Rev. B **22**, 2560 (1980)
24. C. Vanderzande, J.F. Marko, J. Phys. A **26**, 7391 (1993)
25. A. Aharony, G. Ahlers, Phys. Rev. Lett. **44**, 782 (1980)
26. M.P.M. den Nijs, Phys. Rev. B **27**, 1674 (1983)
27. Y. Gefen, B.B. Mandelbrot, A. Aharony, A. Kapitulnik, J. Stat. Phys. **36**, 827 (1984); B.B. Mandelbrot, Y. Gefen, A. Aharony, J. Peyriere, J. Phys. A **18**, 335 (1985)
28. M.E.J. Newman, R.M. Ziff, Phys. Rev. Lett. **85**, 4104 (2000)
29. J. Hoshen, R. Kopelman, Phys. Rev. B **14**, 3438 (1976)
30. W.H. Press, S.A. Teukolsky, W.T.V.B.P. Flannery, *Numerical Recipes in C: The Art of Scientific Computing* (Cambridge University Press, Great Britain, Cambridge, 1992)
31. A. Coniglio, Phys. Rev. Lett. **62**, 3054 (1989)